Brain Stimulation 18 (2025) 800–809

Contents lists available at ScienceDirect

Brain Stimulation

journal homepage: www.journals.elsevier.com/brain-stimulation

Investigating brain network dynamics in state-dependent stimulation: A concurrent electroencephalography and transcranial magnetic stimulation study using hidden Markov models

Saeed Makkinayeri [a], Roberto Guidotti [a,b], Alessio Basti [h], Mark W. Woolrich [c,d], Chetan Gohil [c,d], Mauro Pettorruso [a,b], Maria Ermolova [f], Risto J. Ilmoniemi [e], Ulf Ziemann [f,g], Gian Luca Romani [b], Vittorio Pizzella [a,b,1], Laura Marzetti [b,h,*,1]

[a] Department of Neuroscience, Imaging and Clinical Sciences, G. d'Annunzio University of Chieti-Pescara, Chieti, Italy
[b] Institute for Advanced Biomedical Technologies, G. d'Annunzio University of Chieti-Pescara, Chieti, Italy
[c] Oxford Centre for Human Brain Activity, Wellcome Centre for Integrative Neuroimaging, University of Oxford, Oxford, United Kingdom
[d] Department of Psychiatry, Warneford Hospital, Oxford, Oxford, United Kingdom
[e] Department of Neuroscience and Biomedical Engineering, Aalto University, Espoo, Finland
[f] Department of Neurology & Stroke, University of Tübingen, Tübingen, Germany
[g] Hertie Institute for Clinical Brain Research, University of Tübingen, Tübingen, Germany
[h] Department of Engineering and Geology, G. d'Annunzio University of Chieti-Pescara, Pescara, Italy

ARTICLE INFO

Keywords:
Resting state networks
Electroencephalography
Transcranial magnetic stimulation (TMS)
Motor evoked potential (MEP)
Corticospinal excitability
Network-based stimulation

ABSTRACT

Background: Systems neuroscience studies have shown that baseline brain activity can be categorized into large-scale networks (resting-state-networks, RNSs), with influence on cognitive abilities and clinical symptoms. These insights have guided millimeter-precise selection of brain stimulation targets based on RSNs. Concurrently, Transcranial Magnetic Stimulation (TMS) studies revealed that baseline brain states, measured by EEG signal power or phase, affect stimulation outcomes. However, EEG dynamics in these studies are mostly limited to single regions or channels, lacking the spatial resolution needed for accurate network-level characterization.
Objective: We aim at mapping brain networks with high spatial and temporal precision and to assess whether the occurrence of specific network-level-states impact TMS outcome. To this end, we will identify large-scale brain networks and explore how their dynamics relates to corticospinal excitability.
Methods: This study leverages Hidden Markov Models to identify large-scale brain states from pre-stimulus source space high-density-EEG data collected during TMS targeting the left primary motor cortex in twenty healthy subjects. The association between states and fMRI-defined RSNs was explored using the Yeo atlas, and the trial-by-trial relation between states and corticospinal excitability was examined.
Results: We extracted fast-dynamic large-scale brain states with unique spatiotemporal and spectral features resembling major RSNs. The engagement of different networks significantly influences corticospinal excitability, with larger motor evoked potentials when baseline activity was dominated by the sensorimotor network.
Conclusions: These findings represent a step forward towards characterizing brain network in EEG-TMS with both high spatial and temporal resolution and underscore the importance of incorporating large-scale network dynamics into TMS experiments.

1. Introduction

Systems neuroscience studies have shown that baseline brain activity involves a coordinated interplay among different regions within various brain networks. These networks have primarily been identified with functional Magnetic Resonance Imaging (fMRI) [1–4], but also with Near Infrared Spectroscopy [5,6], Magnetoencephalography (MEG) [7,8], and Electroencephalography (EEG) [9]. In fMRI, baseline brain

* Corresponding author. Institute for Advanced Biomedical Technologies, G. d'Annunzio University of Chieti-Pescara, Chieti, Italy.
E-mail address: laura.marzetti@unich.it (L. Marzetti).
[1] Equal contributions.

https://doi.org/10.1016/j.brs.2025.03.020
Received 2 December 2024; Received in revised form 16 March 2025; Accepted 27 March 2025
Available online 30 March 2025

networks have been denoted as Resting State Networks (RSNs) [1,4,10], and have been shown to support a broad range of cognitive functions [11,12]. Alteration or disruptions in RSNs are frequently linked to clinical symptoms observed in conditions such as depression [13,14], schizophrenia [15,16], neurodegenerative diseases [17,18], aging [19,20], and stroke [21–24]. These findings have also played a crucial role in the design of rehabilitation protocols and in assessing behavioral recovery [25,26].

Along this line, recent advances in brain stimulation have relied on fMRI defined RSNs for target selection for both invasive [27,28] and non-invasive procedures [29–31] with high spatial resolution. This precision seems critical for enhancing the effectiveness of Transcranial Magnetic Stimulation (TMS) [30,32]. In parallel, concurrent EEG and TMS (EEG-TMS) have provided evidence that treatment efficacy is also linked to temporal aspects of the stimulation [33,34].

Indeed, EEG-TMS studies have shown that the brain states at the time of stimulation have a significant impact on the TMS outcome [35,36]. For instance, the amplitude of motor-evoked potentials (MEPs) evoked by the stimulation of the primary motor cortex, a measure of corticospinal excitability, is closely linked to both power [34,37] and phase [35,36,38] of the μ-rhythm. Nevertheless, most of what has been said on the relation between brain state and stimulation outcome derives from a definition of brain state that relies on local/regional properties, i.e., signals from specific regions or EEG channels, usually near the stimulation site. This narrow focus restricts our ability to grasp the broader, more complex interactions occurring across large-scale brain networks.

Functional connectivity approaches with EEG have only very recently been used as brain-state indicators for stimulation timing [39,40]. Nevertheless, EEG functional connectivity studies have been limited to sensor-level data with focus on few a priori selected electrodes, thus exhibiting limited spatial accuracy compared to fMRI network-based stimulation studies.

To leverage the high temporal resolution of EEG-TMS, and, at the same time to exploit the network-based stimulation approach, studies based on high-density EEG and data-driven network analysis approaches are desirable. A promising strategy is to adopt a Hidden Markov Model (HMM) approach [8,41] to extract large-scale brain states and examine their role in modulating TMS responses.

HMMs have been applied across various neuroimaging modalities, including, MEG [7,8], fMRI [2,42] and EEG [43,44] to characterize large-scale brain network dynamics. So far with EEG-TMS data, HMMs applied to the EEG part have been used to extract the burst of neuronal oscillations within motor areas [45] as well as to transfer large-scale brain states from resting-state EEG into EEG-TMS data [46]. Additionally, these studies have explored state-locked modulations of brain oscillations, as a proxy for cortical excitability. While these studies have importantly shown the feasibility of using an HMM-based approach to investigate states-locked modulations of cortical excitability, none of them extracted whole-brain HMM derived brain states from EEG-TMS. More importantly, none of them related HMM output to brain networks and, specifically, to fMRI defined RSNs in order to fill the gap between what is currently known of network-based stimulation targeting and of stimulation timing based on brain-state dynamics.

In this study, we extracted broadband large-scale transient brain states, using HMM, from high density EEG data recorded simultaneously to TMS in the time interval prior to the stimulation of the left primary motor cortex, while measuring Motor Evoked Potentials (MEPs) at the contralateral hand. For this purpose, we identified brain states from source reconstructed pre-stimulus segments of EEG-TMS data. The association between the inferred states and RSNs was explored using the Yeo atlas as a reference. Moreover, we examined how the occurrence of HMM derived large-scale networks before the stimulation relates to corticospinal excitability, comparing the temporal and spectral characteristics of states to understand the relationship between brain dynamics and modulations of MEP amplitude.

2. Material and methods

A schematic version of the materials and methods is provided in Fig. 1 and a detailed description in Supplementary Material S1.

2.1. Participants and experiment

EEG-TMS data were acquired at the University of Tübingen in a group of 20 right-handed individuals (12 females, 8 males; age: 27 ± 4 years, M±1SD). None of the participants had any prior history of neurological and/or psychiatric disorders. All participants gave written informed consent and completed the protocol. The study was approved by the ethical committee of the Medical Faculty of the University of Tübingen (716/2014BO2) and was conducted in accordance with the Declaration of Helsinki.

In a EEG-TMS setup, EEG data were acquired with a 128-channel cap with a sampling rate of 5 kHz. Biphasic pulses were delivered through a figure-of-eight-coil to the hand representation of left primary motor (M1) area with posterior-lateral to anterior-medial orientation. EMG signals were recorded simultaneously at 5 kHz from the abductor pollicis brevis (APB) and the first dorsal interosseous (FDI) muscles of the right hand in a bipolar belly-tendon montage.

In 12 subjects, the experiment was divided into four sessions with a total of 300 pulses delivered in each session (i.e., 1200 in total per subject) and the interstimulus interval was set to 3.00 ± 0.50 s; whilst, in the rest of the cohort, used also in Refs. [40,47], the experiment was done all at once by delivering either 1000 or 1200 pulses (in 3 and 5 subjects, respectively) with interstimulus interval of 2.00 ± 0.25 s. The stimulation intensity was set at 110 % of resting motor threshold [48] for each participant (see supplementary S1.1).

2.2. Preprocessing EEG and EMG

This step involved preprocessing of pre-stimulus part of EEG-TMS data (from −1500 to −10 ms time-locked to TMS) and extracting peak-to-peak MEP amplitudes from the EMG data (see supplementary S1.2).

2.3. Source reconstruction

The source model corresponded to a three-dimensional 6-mm-spaced grid in the Montreal Neurological Institute (MNI) space (9270 vertices). Spatial filters were obtained through the solution of the inverse problem using a scalar array-gain Linearly Constrained Minimum Variance (LCMV) beamformer [49]. The estimated spatial filters were applied to the EEG sensor data to obtain the source activity for an isotropic grid of dipoles spaced 6 mm apart (see supplementary S1.3).

2.4. Parcellation, leakage correction and dipole alignment

To reduce the dimensionality of dipole time courses, a parcellation scheme was applied using the AAL atlas [50]. Seventy-eight parcels were used to cover the entire cortical surface (Supplementary Material Table S1) [53,54]. Principal component analysis was applied to the dipole time courses assigned to a parcel. A symmetric orthogonalization technique [51] was then applied to the parcel time courses to reduce the possibly artefactual zero-lag coupling among them.

Moreover, a random search algorithm [55] was used to align the sign of the parcel time courses across subjects (see supplementary S1.4).

2.5. State inference through hidden markov models

An HMM approach was used to characterize the brain states at group level by isolating distinct spatiotemporal patterns of neuronal oscillations in the parcel signal [56].

For each subject, we concatenated data across trials and then

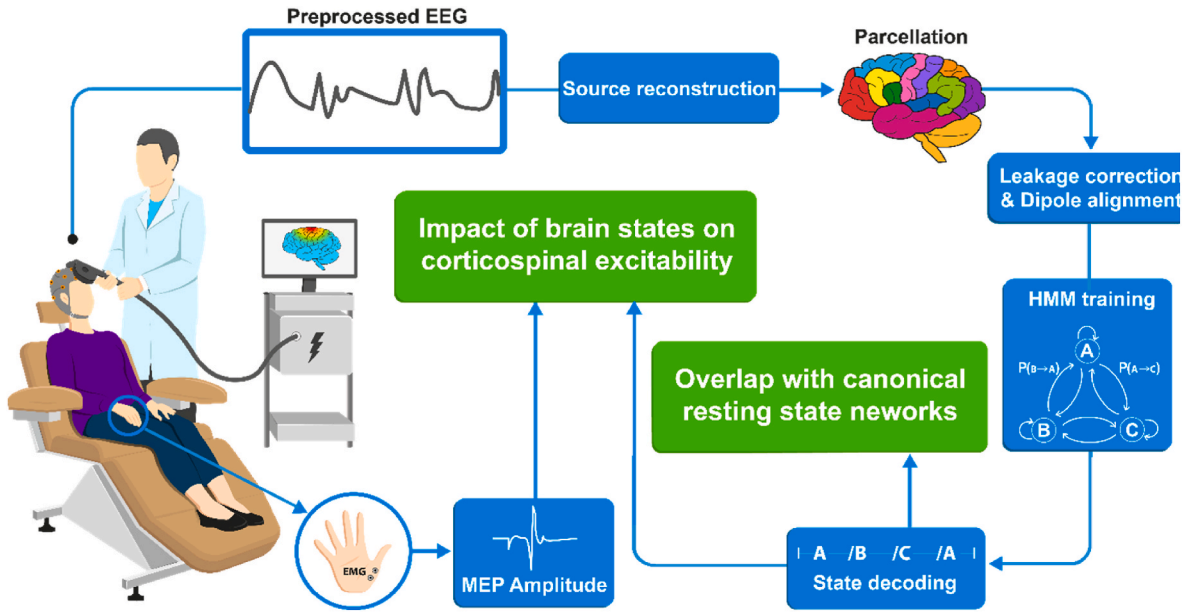

Fig. 1. Diagram of the analysis pipeline. First, the pre-stimulus part of EEG-TMS data was extracted and then preprocessed. Source time series were obtained using the Linearly Constrained Minimum Variance (LCMV) beamforming technique [49]. Parcellation was applied to the source dipoles using the Automated Anatomical Labelling (AAL) atlas [50]. To compensate for volume conduction effects, a symmetric orthogonalization approach [51] was employed. Afterwards, source polarities were aligned across subjects. HMM was trained with a pre-defined number of states, and state sequences were extracted. States power topographies were compared to RNSs of the Yeo atlas [52]. A unified measure of corticospinal excitability was derived from MEP amplitudes of both the right FDI and APB muscles using the first principal component. Finally, the effects of pre-stimulus brain states on corticospinal excitability were assessed using rmANOVA.

standardized (z-transformed) the parcel-level pre-stimulus time courses. We used the time-delayed embedded (TDE)-HMM, which is capable of detecting fast transient brain states that are characterized by distinct spectral properties [8]. Moreover, we used stochastic variational inference to train the HMM on the TDE data [57] (see supplementary S1.5).

After training, the Viterbi algorithm was used to obtain the brain state time series indicating the brain state occurring at each time-point [7]. Temporal summary measures of the states, such as fractional occupancy (FO), lifetime, and interval time were extracted from the inferred state time series [7]. FO was determined by calculating the proportion of time a state was observed, whereas lifetime and interval time quantify the consecutive occurrences of a state and the duration between its reappearance after transitioning to another state. States identified by the TDE-HMM approach will be, in the following, termed Fast-Dynamic Large-Scale Brain States (FLBSs) in line with Marzetti et al., 2024b [58].

2.6. Identification of the number of FLBSs and their robustness

Choosing the optimal number of FLBSs is a fundamental preliminary step. Two metrics, reproducibility of HMMs [8,42,44] and avoidance of sporadic FLBSs [42], were used to assess this number. The former means that the same FLBSs can be observed across different repetitions, while the latter favors FLBSs that appear more often over time and subjects.

Furthermore, control analyses were performed to check subject-dependency of the detected FLBSs, since this dependency could affect the inference process [8,42] (see supplementary S1.6).

2.7. Spectral analysis

Spectral features of FLBSs were analyzed by employing a multi-taper approach (see Ref. [55] for details) to calculate the power spectral density (PSD) and orthogonalized coherence magnitude, referred to as coherence (COH) in following, spectrum across a frequency range of 3–30 Hz. We then averaged these values within specific frequency bands of interest—broadband (3–30 Hz), theta (3–8 Hz), alpha (8–13 Hz), and beta (13–30 Hz)—to determine the power and coherence characteristics of the FLBSs in these bands.

2.8. Correspondence of FLBSs to canonical Resting State Networks

To quantify the similarity between our FLBSs and canonical RSNs, we used the Dice Overlap Coefficient (DOC), ranging from 0 (no spatial correspondence) to 1 (total spatial correspondence) as implemented in the Network Correspondence Toolbox [59]. The Yeo atlas [52] served as the reference template (see supplementary S1.8).

2.9. Statistical analyses

Statistical differences between lifetime, interval time and FO of the brain FLBSs were investigated separately using one-way repeated measure of ANOVA (rmANOVA).

The FLBSs duration at the time of stimulation was divided into two groups based on the median value: short- and long-lasting FLBSs. A two-way rmANOVA was conducted to examine the effects of FLBSs (nine levels: FLBS1-FLBS9) and the duration of FLBSs (two levels: short-lasting and long-lasting) on MEP amplitude. The aim was to determine whether significant differences in MEPs existed due to the occurrence of specific FLBSs and the duration of FLBSs at the time of stimulation, as well as to explore interactions between the FLBS visit durations and occurrences (see supplementary S1.9).

3. Results

Our approach to estimate the number of FLBSs, based on having a reproducible model alongside limiting visits to sporadic FLBSs, resulted in inferring nine FLBSs (Supplementary Fig. S1). Further, subject-dependency analysis confirmed that the extracted FLBSs are robust to subject variability (Supplementary Fig. S2).

3.1. TDE-HMM identifies distinct resting-state networks in pre-stimulus EEG-TMS

The large-scale spatial distributions of broadband power and coherence, for six out of the nine estimated FLBSs (i.e. brain states) are displayed in Fig. 2. Supplementary Fig. S3 provides information on the power and coherence of the remaining FLBSs.

The six FLBSs exhibit distinct and bilaterally symmetric patterns of power and coherence across cortical areas, except for FLBS1. FLBS1 represents a network predominantly activated in the right hemisphere, including the superior medial frontal, inferior frontal, middle frontal, and superior temporal regions. This topography aligns with Default Mode Network (DMN) and Control Network (CN). FLBS2 encompasses the medial and inferior frontal regions (IFG), middle temporal gyrus (MTG), temporal pole (TPO), and the anterior and posterior cingulate gyri (ACG and PCG), overlapping with DMN.

FLBS3 is characterized by bilateral precentral (PreCG) and post-central gyrus (PoCG) nodes, aligning with the Sensorimotor Network (SMN). FLBS4, dominated by activation in the precuneus (PCUN), superior parietal gyrus (SPG), and middle visual cortex, is associated to Visual Network (VN). FLBS5 includes contributions from the parietal regions, PreCG, and PoCG, suggesting similar pattern to Dorsal Attention Network (DAN). Finally, FLBS6 captures activation in the visual cortex and overlaps with VN.

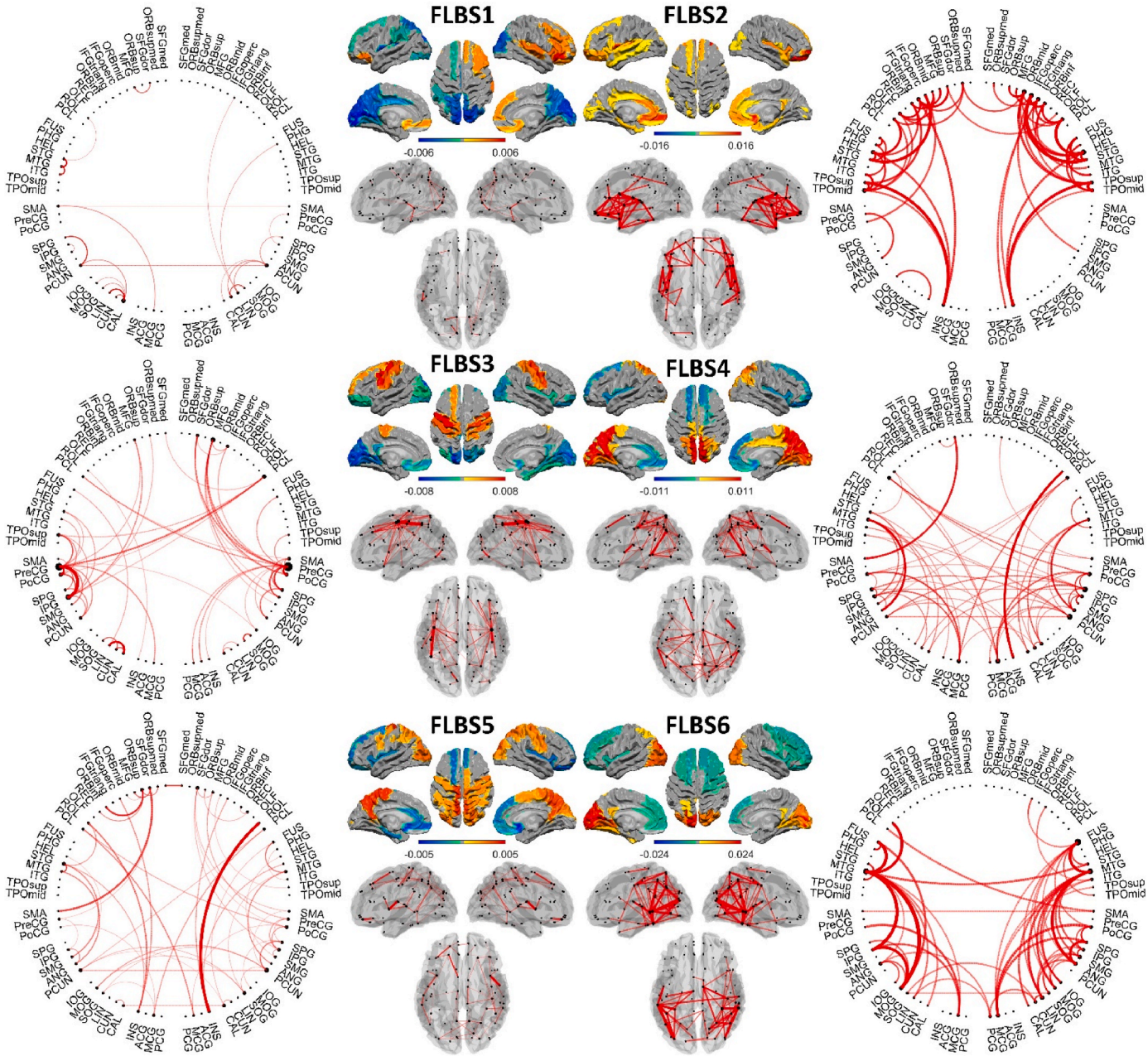

Fig. 2. Spatial broadband power and coherence of the six FLBSs (i.e. brain states). The positive values in the power map indicate values above the FLBS average power across parcels, while negative values are below this average. For visualization, only the top 40 % of positive and negative values are shown. For coherence, the strongest FLBS connections were identified using a two-component Gaussian mixture model and the top 1 % of FC values from the higher mean Gaussian are shown. The thickness of the lines indicates the relative strength of the connections, while the size of the nodes is the relative degree measure (see supplementary S2). FLBS1 represents DMN and CN; FLBS2 overlaps with DMN; FLBS3 corresponds to SMN. Both FLBS4 and FLBS6 are associated with VN, while FLBS5 overlaps with DAN. DMN = Default mode network, CN = Control network, VN Visual network, DAN = Dorsal attention network.

3.2. Differences in temporal characteristics of FLBSs highlight a short-lived and reoccurring nature of brain dynamics

Brain dynamics are characterized by temporal features such as lifetime, interval time, and FO (Fig. 3A–C). The average lifetime significantly differs among the FLBSs ($F_{(3.45,65.7)} = 13.50, p < 0.001$), ranging from 78.9 ms in FLBS7 to 135.4 ms in FLBS9, with the total average lifetime of 99.7 ms, indicating that the FLBSs are generally short-lived. Differences in the interval times between FLBSs are also significant ($F_{(3.09,58.87)} = 77.72, p < 0.001$). The total average interval time of FLBSs is 0.9 s, while they vary from 0.4 s in FLBS1 to 2.9 s in FLBS2, showcasing the reoccurring nature of FLBSs. Additionally, FLBSs exhibit significantly different FO ($F_{(3.42,64.98)} = 6.82, p < 0.001$). FLBS2 displays the lowest average FO at 3.7 %, whereas FLBS9 has the highest at 16.7 %. The distribution of FO across subjects (Fig. 3D) indicates that maximum FO ranges from 19.2 % to 50.1 %. Meanwhile, minimum FO across subjects range from 1.0 % to 4.5 %, demonstrating that all FLBSs are present in all subjects and are not biased by subject differences.

3.3. FLBSs exhibit different spectral and connectivity signatures

Fig. 4A–B illustrate the average PSD and COH across brain regions at all the frequencies. The black line and shaded areas represent the mean and standard error across all FLBSs. The average PSD and average COH of the remaining FLBSs are depicted in Supplementary Fig. S6. Additionally, due to the importance of PreCG, which is the stimulation site in our study, a detailed assessment of PSD and total COH in both the left and right PreCG are depicted in Fig. 4C–F.

FLBS2, primarily dominated by theta oscillations, stands out with the highest average power and coherence across all the frequency bands except for coherence in the alpha band. Moreover, FLBS6 demonstrates above-average power and the highest coherence in the alpha band. The average PSD of FLBS1 characterized by theta frequency, while its average COH peaks in the early alpha rhythms (~8Hz). The average PSD and COH of the remaining three FLBSs predominantly exhibit alpha oscillations. Notably, FLBS5 and FLBS1 have the lowest average power and coherence in the three frequency bands, respectively.

FLSB3 demonstrates the highest power within the alpha and beta frequency bands bilaterally in PreCG (Fig. 4C–E). Conversely, FLBS2 exhibits the highest power in the theta band. On the other hand, FLBS6 displays the lowest power within both regions in the theta and beta bands, while FLBS1, FLBS5, and FLBS6 exhibit nearly identical, lowest power levels in the alpha band. FLBS2 exhibits stronger total coherence in the theta and beta rhythms across both gyri (Fig. 4D–F). However, the highest total coherence in the alpha band is observed in FLBS3 within the left PreCG and in FLBS6 within the right PreCG. FLBS1 displays the lowest total coherence for both regions across all frequency bands.

3.4. Brain states characteristics show relationship with corticospinal excitability

For each FLBS (i.e. brain state), we tested the hypothesis that the rate of FLBS occurrence and the duration of FLBS visit, impacts MEP amplitude at the time of stimulation, using a two-way repeated measures ANOVA (rmANOVA). We also tested the impact of the interaction between the rate of occurrence and duration. To test the impact of the duration of FLBS visits, we divided all the trials into two groups based on the median duration (80 ms): long-lasting (larger than the median) and short-lasting (80 ms or less) (Fig. 5A). A significant main effect of FLBSs on MEPs is observed ($F_{(8,152)} = 2.05, p < 0.01, \eta^2 = 0.10$), Although the other main effect, the FLBS visit duration, does not yield significant difference in MEP amplitude ($F_{(1,19)} = 2.01, p > 0.05, \eta^2 = 0.10$). The interaction effect between FLBSs and the FLBS visit duration is significant, $F_{(8,152)} = 2.06, p < 0.05, \eta^2 = 0.10$. The post-hoc analysis (paired-sample t-tests) of the main effect of FLBSs (Fig. 5B) indicates that there is a significant difference between FLBS3 (M±1SE, 7.24 ± 2.31 %) and FLBS4 (M±1SE, −9.89 ± 2.85 %) ($t = 4.75, p < 0.01$). No significant difference between short-lasting FLBSs is found (Fig. 5C). However, MEPs modulated by long-lasting FLBS3 (M±1SE, 14.55 ± 3.99 %) are significantly larger in average than the ones modulated by long-lasting FLBS4 (M±1SE, −13.02 ± 3.69 %) ($t = 5.24, p < 0.01$) (Fig. 5D). The other significant difference is seen between long-lasting FLBS3 and long-

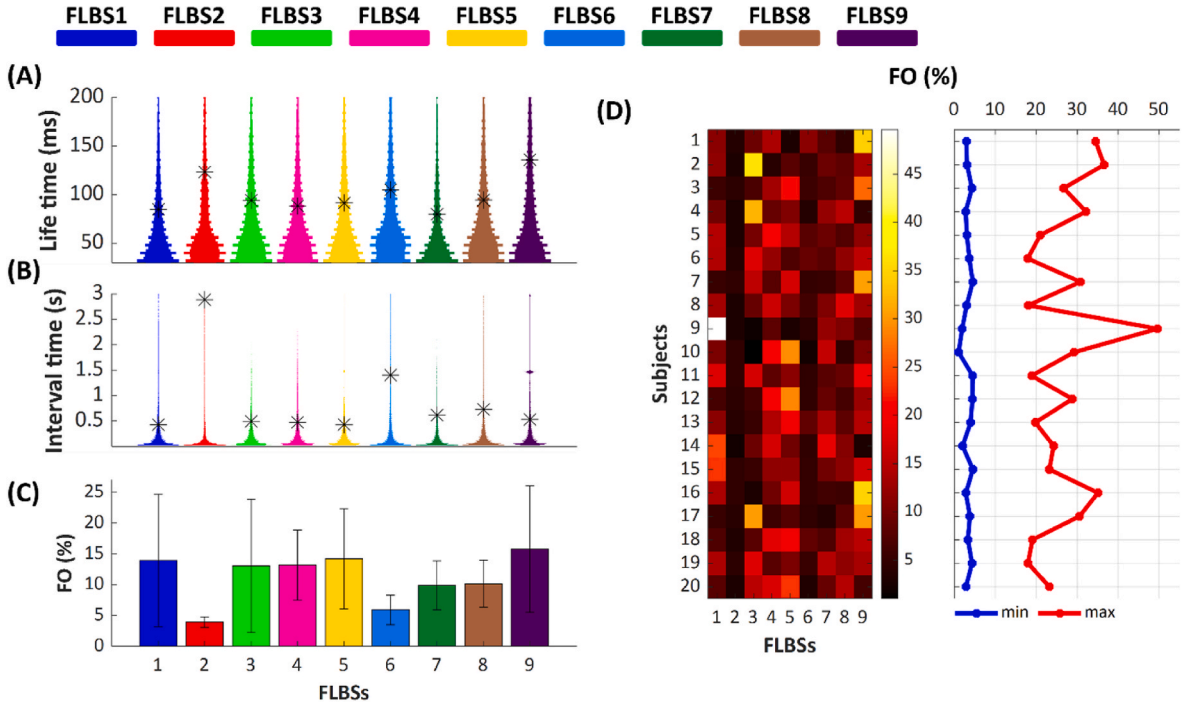

Fig. 3. (A) Lifetime, (B) interval time, and (C) fractional occupancy (FO). The FLBSs last on average 99.7 ms, while they reoccur every 0.9 s, on average. The average FO of the FLBSs vary from 3.7 % up to 16.7 %. (D) indicates that all FLBSs are present in all subjects.

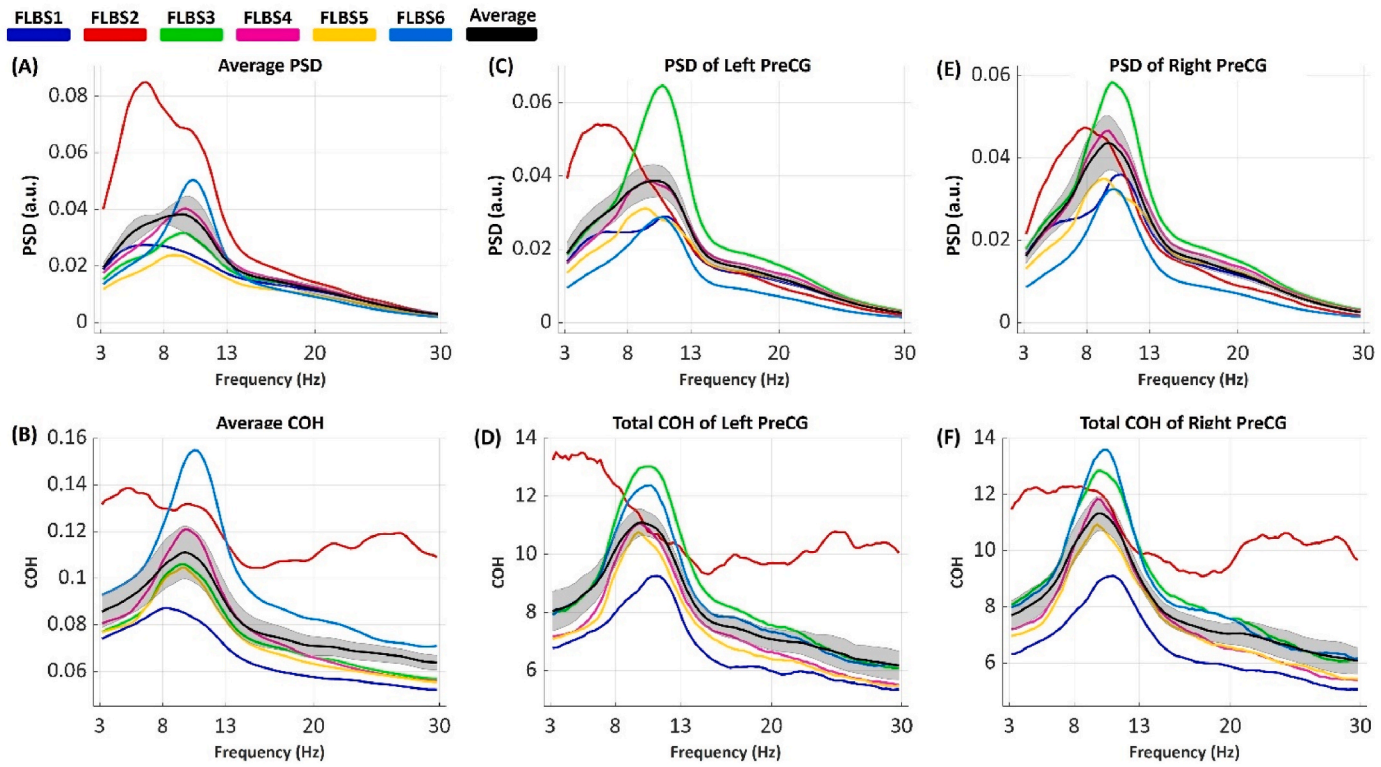

Fig. 4. (A–B) PSD and COH of the FLBSs averaged across regions. The black line and shaded area denote the overall average and standard deviation. FLBS1 and FLBS2 are primarily characterized by theta oscillations (4–8 Hz), while the other four FLBSs predominantly exhibit alpha (8–13 Hz) oscillations. (C–F) PSD and total COH of the left and right PreCG are visualized, revealing that FLBS3 shows the highest power in both gyri in the alpha and beta rhythms (13–30 Hz). Additionally, FLBS3 demonstrates the highest total coherence in the alpha rhythm of left PreCG.

lasting FLBS6 (M±1SE, -7.26 ± 4.42 %), ($t = 4.54$, $p < 0.01$). Fig. 5E depicts the subject-wise MEP modulations for FLBS3 as a responsive FLBS and the average MEPS of FLBS4 and FLBS6 as non-responsive FLBSs. In 18 subjects out of 20, FLBS3 indexes larger or equal MEPs compared to the average MEPs of FLBS4 and FLBS6, although in two subjects, MEP modulations are lower. Additionally, the group-level comparison using paired-sample t-tests reveals a significant difference between MEPs of long-lasting FLBS3 and the average FLBS4 and FLBS6 ($t = 5.75$, $p < 0.001$).

4. Discussion

Perturbational approaches targeting fMRI-defined networks have shown better performance in modulating behavior or symptoms. In addition, TMS informed by brain dynamics from EEG has been instrumental to induce plastic changes in the central nervous system compared to non-EEG-informed TMS. Here, we aimed at extracting EEG-networks with spatial correspondence to fMRI-networks and with a fast dynamic in light of a paradigm shift towards dynamical-network-based stimulation. To this end, we delivered TMS to the primary motor cortex, while recording high-density-EEG, to investigate peripheral responses in a dynamical-network-based stimulation framework. We observe large overlap of EEG networks with Default Mode, Dorsal Attention, Sensorimotor, and Visual networks, and a unique relation to trial-by-trial MEP amplitude.

Specifically, we investigated the impact of fast-changing broadband large-scale pre-stimulus brain states on corticospinal excitability using the TDE-HMM [8]. Our analysis demonstrates that, while there is no definitive “correct" number of states - fewer states capture broader aspects, whereas a higher number reveals more detailed network structures [8,55] - the TDE-HMM could successfully identify nine distinct brain states in the pre-stimulus EEG-TMS data with unique spectral, temporal, and spatial features. We refer to these brain states as Fast-Dynamic Large-Scale Brain States (FLBSs) [58].

The HMM has been used to study brain dynamics in neuroimaging contexts, including resting state [2,7,8,57], task-based [55,57,60], sleep [42], and burst identifications [43,61]. In this study, TDE-HMM revealed transient FLBSs with an average lifetime of 99.7 ms (Fig. 3A), which is consistent with MEG studies [8]. Moreover, the average interval time of 0.9 s (Fig. 3B), guaranteed the reoccurrence of FLBSs throughout the data. The distribution of FO across subjects (Fig. 3D) indicates that the identified FLBSs are not biased by between-subject differences, suggesting that the model captures dynamic rather than static (time-averaged) functional connectivity (FC) patterns [62].

Moreover, each FLBS shows similarities with even more than one well-known resting-state networks activity pattern that has been observed in fMRI [1,63] (Fig. 2). This might be due to the limiting assumption of mutual exclusivity of HMM [8,44,55], positing that only one state can occur at any given time. This constraint may amalgamate patterns from different networks, preventing the detection of co-activation or co-inactivation of multiple states. Alternative methods, including Recurrent Neural Networks (RNNs) and Long-Short Term Memory, are progressively being applied to capture the intrinsic characteristics of brain signals and infer hidden states [80–83]. A recent study by Gohil et al. [77] introduced a RNN-based model called DyNeMo (Dynamic Network Modes), which relaxes the mutual exclusivity constraint and models functional connectivity as a dynamic mixture of network modes. Unlike HMM, DyNeMo can capture simultaneous activation of multiple states and long-range temporal dependencies. However, the findings suggest that the assumption of mutual exclusivity made by HMM remains valid in practical applications. Future research may take advantage of DyNeMo or other approaches to further explore alternative state-space models [84], providing deeper insights into the temporal dynamics of neural activity and complex brain state

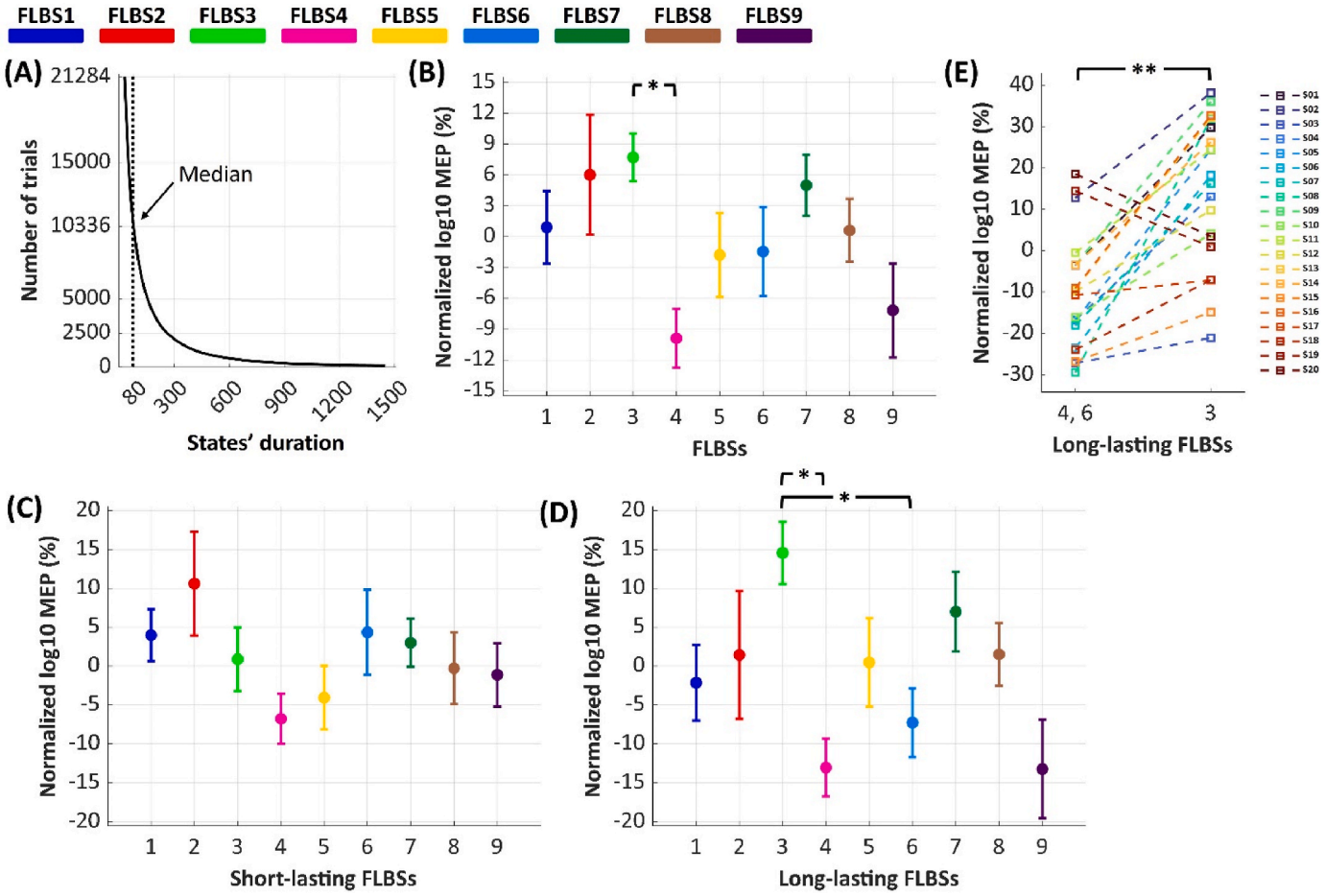

Fig. 5. (A) Visits to each FLBS at the time of stimulation are categorized into long-lasting and short-lasting groups based on 80-ms-duration. A two-way rmANOVA was conducted to investigate the main effects of FLBSs and their visit durations at the time of stimulation, as well as their interaction. (B) The result indicates that MEP amplitudes are significantly influenced by FLBSs. Post-hoc analysis revealed a significant difference among FLBS3 (SMN) and FLBS4 (VN). Additionally, the interaction between FLBSs and their visit durations significantly affects MEP variability. (C) Post-hoc analysis shows no significant differences among short-lasting FLBSs. (D) However, significant differences between long-lasting FLBS3 and FLBS4, as well as between FLBS3 and FLBS6 are observed ($*p < 0.01$). (E) Subject-level average MEP modulations for FLBS4 and FLBS6 and MEPs of FLBS3 ($**p < 0.001$).

interactions.

Despite this possible limitation, FLBS4 and FLBS6 demonstrate clear patterns of activity corresponding to the visual network, characterized by alpha rhythm [64,65], while FLBS3 captures SMN alpha and beta oscillations, consistent with established studies [66]. FLBS2 exhibits behavior akin to DMN, a task-negative network involved in self-referential and mind-wandering activities [67,68] with medial prefrontal cortex (mPFC) and PCG serving as key regions. This DMN-like state is predominantly characterized by theta rhythm, corroborating previous research [8]. FLBS5 appears to correspond to DAN, a symmetric network involving the bi-hemispheric intraparietal sulcus and frontal eye fields located in the precentral sulcus [69], oscillating in the alpha rhythm. Finally, FLBS1, though less clear, aligns with DMN and CN. Given the presence of the right inferior frontal region, it might correspond to the inhibitory task of the control executive network [70, 71].

Previous studies have demonstrated that stimulating a region when its corresponding large-scale network is active enhances cortical excitability. This effect has been observed in large-scale visual, parietal networks during TMS [46] as well as in the motor network [72]. These studies indicate that stimulation coinciding with the active state of a network may lead to increased cortical and corticospinal excitability. Our findings corroborate this evidence since we found a statistical dependency between large-scale brain networks and corticospinal excitability. Specifically, our findings indicate that MEPs are significantly larger when the long-lasting SMN (FLBS3) is active at the time of stimulation compared to when FLBS4 or FLBS6 are active. This suggests that the state of the pre-stimulus neuronal network plays a crucial role in modulating corticospinal excitability, highlighting the importance of the motor network in enhancing motor responses.

FLBS4 and FLBS6 exhibit enhanced power in visual areas, while FLBS3 shows reduced power in the same areas, suggesting an anti-correlation between the motor network and the level of alpha visual activity. This is in line with previous studies, showing that alpha power in the visual cortex is positively associated with the attention system [65], while alpha power decreases with increased attention [66,73], potentially explaining the significant difference in MEP amplitudes. Additionally, the observed differences in MEPs between short-lasting and long-lasting states suggest that the brain may require sufficient time to transition into an excitable or inhibitable state. This temporal requirement could account for why long-lasting states yield significant results in terms of MEP amplitudes.

In a previous proof-of-concept study, we performed an HMM analysis in sensor space on eight subjects from this cohort, successfully identifying distinct patterns [58]. Among these patterns the sensor-level correspondent of the sensorimotor and of the visual networks were detected and exhibited a relation to MEP amplitude that is in line with the findings reported in the present work. However, given that volume conduction may negatively influence sensor-level findings, we here pursued a source-level analysis. Given that any approach relying on an

inverse solution is inherently subject to uncertainties, our source-level approach has been optimized through the use of beamformers, parcellation, orthogonalization techniques in line with the robust pipeline successfully applied in multiple previous studies [57,76–79].

Finally, it should be noted that brain states extracted using the TDE-HMM approach capture both power-envelope co-modulations among different brain regions and temporal consistency of phase-locking in band-limited oscillatory signals [8]. In essence, TDE-HMM identifies states based on the two fundamental brain coupling mechanisms: envelope-coupling and phase-coupling [74].

In some scenarios, there might be overlap between local measures and TDE-HMM state. For instance, a locally high-power state may co-occur with a remote high-power state, creating power co-modulation, and a corresponding functional state captured by HMM. In another case, a specific phase of local oscillations may be mirrored at a distant brain region, creating phase-locking, and a corresponding functional state captured by HMM. Thus, while TDE-HMM states are fundamentally different from local measures, certain conditions may result in overlapping observations across approaches, with the HMM approach embedding also the local feature. For example, in our results, FLBS3 exhibited high oscillatory power in L PreCG, suggesting that local power fluctuations may contribute to its characterization. This aligns with prior findings showing that M1 mu-rhythm power is positively associated with corticospinal excitability [34,35,37,75]. Moreover, it has been shown that functional connectivity of M1 correlates positively with MEP amplitude [39,40], a relationship also observed in our results, as FLBS3 was associated with stronger connectivity within the motor network. This highlights the advantage of the HMM-based approach over traditional single-region EEG markers by integrating both local power and broader network dynamics, offering a broader perspective on brain state-dependent stimulation.

Future research can leverage the HMM's ability to capture fast-changing brain states to differentiate neural dynamics between populations, such as healthy individuals and those with neuropsychiatric disorders. HMM has already been applied in major depressive disorder (MDD), revealing disruptions in brain dynamics [85,86], as well as in infants, where perinatal brain injury was found to prolong state lifetimes and reduce sleep state flexibility [44]. Additionally, HMM analysis of magnetoencephalographic data in multiple sclerosis has provided insights into disease-specific and treatment-related changes in task-relevant networks [87]. HMM-derived brain state markers could help optimize neuromodulation strategies, addressing the variable efficacy of rTMS in neuropsychiatric disorders. State-dependent stimulation, such as alpha-synchronized rTMS in MDD [88], has shown potential in modulating abnormal neural oscillations [89]. Future research could further refine brain state identification, optimize stimulation timing, and enhance rTMS protocols for improved therapeutic outcomes.

Finally, the use of multimodal techniques would allow for a more detailed validation of the spatial and temporal characteristics of the HMM-derived states. fMRI would provide high spatial resolution to identify the specific brain regions involved, while EEG could capture the precise timing of neural activity and dynamic interactions. By integrating these data [90–92], we could gain a more comprehensive understanding of brain state dynamics, enhancing the robustness of HMM and its application in neuromodulation studies.

5. Conclusions

This study demonstrates that the TDE-HMM technique can effectively identify large-scale brain states analogous to canonical fMRI resting-state networks in the pre-stimulus part of an EEG-TMS experiment. The identified states exhibit distinct spatial, temporal, and spectral characteristics. Furthermore, we established a significant association between fast transient large-scale brain networks and corticospinal excitability. Our findings reveal that MEPs are larger when the motor network is more engaged before stimulation, underscoring the critical role of the pre-stimulus neuronal state in modulating corticospinal excitability. These findings serve as a foundation for state-dependent neurostimulation, helping to fill the gap between what is currently known of network-based stimulation targeting and of brain state dynamics.

Declaration of generative AI and AI-assisted technologies in the writing process

During the preparation of this work the authors used ChatGPT 4 in order to improve English language. After using this tool, the authors reviewed and edited the content as needed and take full responsibility for the content of the publication.

Fundings

This research received funding from the European Research Council (ERC Synergy) under the European Union's Horizon 2020 research and innovation programme (ConnectToBrain; grant agreement No. 810377). The content of this article reflects only the author's view, and the ERC Executive Agency is not responsible for the content. L.M. acknowledges financial support of the European Union - Next Generation EU, Mission 4 Component 1 CUP D53D23019260001, Project NEUROSTAR BTP.

CRediT authorship contribution statement

Saeed Makkinayeri: Writing – review & editing, Writing – original draft, Visualization, Software, Methodology, Formal analysis. **Roberto Guidotti:** Writing – review & editing, Methodology. **Alessio Basti:** Writing – review & editing, Methodology. **Mark W. Woolrich:** Writing – review & editing, Methodology. **Chetan Gohil:** Writing – review & editing, Methodology. **Mauro Pettorruso:** Writing – review & editing. **Maria Ermolova:** Writing – review & editing, Investigation. **Risto J. Ilmoniemi:** Writing – review & editing, Funding acquisition. **Ulf Ziemann:** Writing – review & editing, Funding acquisition. **Gian Luca Romani:** Writing – review & editing, Funding acquisition. **Vittorio Pizzella:** Writing – review & editing, Writing – original draft, Supervision, Methodology, Conceptualization. **Laura Marzetti:** Writing – review & editing, Writing – original draft, Supervision, Methodology, Conceptualization.

Declaration of competing interest

The authors declare the following financial interests/personal relationships, which may be considered as potential competing interests: R.J.I. has received consulting fees from Nexstim plc and has patents and patent applications on TMS technology. U.Z. received grants from the German Ministry of Education and Research (BMBF), German Research Foundation (DFG), Takeda Pharmaceutical Company Ltd., and consulting fees from CorTec GmbH, all not related to this work. The other authors declare that they have no known competing financial interests or personal relationships that could have appeared to influence the work reported in this paper.

Acknowledgements

The authors wish to thank Dr. Antonello Baldassarre for helpful discussions.

Appendix A. Supplementary data

Supplementary data to this article can be found online at https://doi.org/10.1016/j.brs.2025.03.020.

References

[1] Damoiseaux JS, et al. Consistent resting-state networks across healthy subjects. Proc Natl Acad Sci USA Sep. 2006;103(37):13848–53. https://doi.org/10.1073/pnas.0601417103.

[2] Vidaurre D, Smith SM, Woolrich MW. Brain network dynamics are hierarchically organized in time. Proc Natl Acad Sci USA Nov. 2017;114(48):12827–32. https://doi.org/10.1073/pnas.1705120114.

[3] Allen EA, Damaraju E, Plis SM, Erhardt EB, Eichele T, Calhoun VD. Tracking whole-brain connectivity dynamics in the resting state. Cerebr Cortex Mar. 2014;24(3):663–76. https://doi.org/10.1093/cercor/bhs352.

[4] Fox MD, Raichle ME. Spontaneous fluctuations in brain activity observed with functional magnetic resonance imaging. Nat Rev Neurosci Sep. 2007;8(9):700–11. https://doi.org/10.1038/nrn2201.

[5] Mesquita RC, Franceschini MA, Boas DA. Resting state functional connectivity of the whole head with near-infrared spectroscopy. Biomed Opt Express Aug. 2010;1(1):324. https://doi.org/10.1364/BOE.1.000324.

[6] Lu C-M, Zhang Y-J, Biswal BB, Zang Y-F, Peng D-L, Zhu C-Z. Use of fNIRS to assess resting state functional connectivity. J Neurosci Methods Feb. 2010;186(2):242–9. https://doi.org/10.1016/j.jneumeth.2009.11.010.

[7] Baker AP, et al. Fast transient networks in spontaneous human brain activity. Elife Mar. 2014;3:e01867. https://doi.org/10.7554/eLife.01867.

[8] Vidaurre D, et al. Spontaneous cortical activity transiently organises into frequency specific phase-coupling networks. Nat Commun Jul. 2018;9(1):2987. https://doi.org/10.1038/s41467-018-05316-z.

[9] Michel CM, Murray MM. Towards the utilization of EEG as a brain imaging tool. Neuroimage Jun. 2012;61(2):371–85. https://doi.org/10.1016/j.neuroimage.2011.12.039.

[10] Deco G, Corbetta M. The dynamical balance of the brain at rest. Neuroscientist Feb. 2011;17(1):107–23. https://doi.org/10.1177/1073858409354384.

[11] Smith SM, et al. Correspondence of the brain's functional architecture during activation and rest. Proc Natl Acad Sci USA Aug. 2009;106(31):13040–5. https://doi.org/10.1073/pnas.0905267106.

[12] Menon V. Large-scale brain networks and psychopathology: a unifying triple network model. Trends Cognit Sci Oct. 2011;15(10):483–506. https://doi.org/10.1016/j.tics.2011.08.003.

[13] Dutta A, McKie S, Deakin JFW. Resting state networks in major depressive disorder. Psychiatry Res Neuroimaging Dec. 2014;224(3):139–51. https://doi.org/10.1016/j.pscychresns.2014.10.003.

[14] Ye M, Yang T, Qing P, Lei X, Qiu J, Liu G. Changes of functional brain networks in major depressive disorder: a graph theoretical analysis of resting-state fMRI. PLoS One Sep. 2015;10(9):e0133775. https://doi.org/10.1371/journal.pone.0133775.

[15] Li P, et al. Altered brain network connectivity as a potential endophenotype of schizophrenia. Sci Rep Jul. 2017;7(1):5483. https://doi.org/10.1038/s41598-017-05774-3.

[16] Hadley JA, Kraguljac NV, White DM, Ver Hoef L, Tabora J, Lahti AC. Change in brain network topology as a function of treatment response in schizophrenia: a longitudinal resting-state fMRI study using graph theory. Npj Schizophr Apr. 2016;2(1):16014. https://doi.org/10.1038/npjschz.2016.14.

[17] Edwards MJ, Yogarajah M, Stone J. Author Correction: why functional neurological disorder is not feigning or malingering. Nat Rev Neurol Jun. 2023;19(6):384. https://doi.org/10.1038/s41582-023-00821-2.

[18] Pievani M, Filippini N, Van Den Heuvel MP, Cappa SF, Frisoni GB. Brain connectivity in neurodegenerative diseases—from phenotype to proteinopathy. Nat Rev Neurol Nov. 2014;10(11):620–33. https://doi.org/10.1038/nrneurol.2014.178.

[19] Wu J-T, et al. Aging-related changes in the default mode network and its anti-correlated networks: a resting-state fMRI study. Neurosci Lett Oct. 2011;504(1):62–7. https://doi.org/10.1016/j.neulet.2011.08.059.

[20] Damoiseaux JS, et al. Reduced resting-state brain activity in the "default network" in normal aging. Cerebr Cortex Aug. 2008;18(8):1856–64. https://doi.org/10.1093/cercor/bhm207.

[21] Tuladhar AM, et al. Default mode network connectivity in stroke patients. PLoS One Jun. 2013;8(6):e66556. https://doi.org/10.1371/journal.pone.0066556.

[22] Zhu Y, Bai L, Liang P, Kang S, Gao H, Yang H. Disrupted brain connectivity networks in acute ischemic stroke patients. Brain Imaging Behav Apr. 2017;11(2):444–53. https://doi.org/10.1007/s11682-016-9525-6.

[23] Baldassarre A, et al. Large-scale changes in network interactions as a physiological signature of spatial neglect. Brain Dec. 2014;137(12):3267–83. https://doi.org/10.1093/brain/awu297.

[24] Urbin MA, Hong X, Lang CE, Carter AR. Resting-state functional connectivity and its association with multiple domains of upper-extremity function in chronic stroke. Neurorehabilitation Neural Repair Oct. 2014;28(8):761–9. https://doi.org/10.1177/1545968314522349.

[25] Grefkes C, Fink GR. Connectivity-based approaches in stroke and recovery of function. Lancet Neurol Feb. 2014;13(2):206–16. https://doi.org/10.1016/S1474-4422(13)70264-3.

[26] Baldassarre A, Ramsey LE, Siegel JS, Shulman GL, Corbetta M. Brain connectivity and neurological disorders after stroke. Curr Opin Neurol Dec. 2016;29(6):706–13. https://doi.org/10.1097/WCO.0000000000000396.

[27] Baldermann JC, et al. Connectivity profile predictive of effective deep brain stimulation in obsessive-compulsive disorder. Biol Psychiatry May 2019;85(9):735–43. https://doi.org/10.1016/j.biopsych.2018.12.019.

[28] Horn A, et al. Connectivity Predicts deep brain stimulation outcome in P arkinson disease. Ann Neurol Jul. 2017;82(1):67–78. https://doi.org/10.1002/ana.24974.

[29] Weigand A, et al. Prospective validation that subgenual connectivity predicts antidepressant efficacy of transcranial magnetic stimulation sites. Biol Psychiatry Jul. 2018;84(1):28–37. https://doi.org/10.1016/j.biopsych.2017.10.028.

[30] Fox MD, Buckner RL, White MP, Greicius MD, Pascual-Leone A. Efficacy of transcranial magnetic stimulation targets for depression is related to intrinsic functional connectivity with the subgenual cingulate. Biol Psychiatry Oct. 2012;72(7):595–603. https://doi.org/10.1016/j.biopsych.2012.04.028.

[31] S. H. Siddiqi et al., 'REpetitive transcranial magnetic stimulation with resting-state network targeting for treatment-resistant depression in traumatic brain injury: a randomized, controlled, double-blinded pilot study'.

[32] Cash RFH, et al. Using brain imaging to improve spatial targeting of transcranial magnetic stimulation for depression. Biol Psychiatry Nov. 2021;90(10):689–700. https://doi.org/10.1016/j.biopsych.2020.05.033.

[33] Ferreri F, Vecchio F, Ponzo D, Pasqualetti P, Rossini PM. Time-varying coupling of EEG oscillations predicts excitability fluctuations in the primary motor cortex as reflected by motor evoked potentials amplitude: an EEG-TMS study. Hum Brain Mapp May 2014;35(5):1969–80. https://doi.org/10.1002/hbm.22306.

[34] Ogata K, Nakazono H, Uehara T, Tobimatsu S. Prestimulus cortical EEG oscillations can predict the excitability of the primary motor cortex. Brain Stimul Nov. 2019;12(6):1508–16. https://doi.org/10.1016/j.brs.2019.06.013.

[35] Bergmann TO, Lieb A, Zrenner C, Ziemann U. Pulsed facilitation of corticospinal excitability by the sensorimotor μ-alpha rhythm. J Neurosci Dec. 2019;39(50):10034–43. https://doi.org/10.1523/JNEUROSCI.1730-19.2019.

[36] Zrenner C, Desideri D, Belardinelli P, Ziemann U. Real-time EEG-defined excitability states determine efficacy of TMS-induced plasticity in human motor cortex. Brain Stimul Mar. 2018;11(2):374–89. https://doi.org/10.1016/j.brs.2017.11.016.

[37] Thies M, Zrenner C, Ziemann U, Bergmann TO. Sensorimotor mu-alpha power is positively related to corticospinal excitability. Brain Stimul Sep. 2018;11(5):1119–22. https://doi.org/10.1016/j.brs.2018.06.006.

[38] Hussain SJ, et al. Sensorimotor oscillatory phase–power interaction gates resting human corticospinal output. Cerebr Cortex Aug. 2019;29(9):3766–77. https://doi.org/10.1093/cercor/bhy255.

[39] Vetter DE, et al. Targeting motor cortex high-excitability states defined by functional connectivity with real-time EEG–TMS. Neuroimage Dec. 2023;284:120427. https://doi.org/10.1016/j.neuroimage.2023.120427.

[40] Marzetti L, et al. Exploring motor network connectivity in state-dependent transcranial magnetic stimulation: a proof-of-concept study. Biomedicines Apr. 2024;12(5):955. https://doi.org/10.3390/biomedicines12050955.

[41] Rezek I, Roberts S. 'Ensemble hidden Markov models with extended observation densities for biosignal analysis', in probabilistic modeling in bioinformatics and medical informatics. In: Husmeier D, Dybowski R, Roberts S, editors. Advanced information and knowledge processing. London: Springer-Verlag; 2005. p. 419–50. https://doi.org/10.1007/1-84628-119-9_14.

[42] Stevner ABA, et al. Discovery of key whole-brain transitions and dynamics during human wakefulness and non-REM sleep. Nat Commun Mar. 2019;10(1):1035. https://doi.org/10.1038/s41467-019-08934-3.

[43] Coquelet N, et al. Microstates and power envelope hidden Markov modeling probe bursting brain activity at different timescales. Neuroimage Feb. 2022;247:118850. https://doi.org/10.1016/j.neuroimage.2021.118850.

[44] Khazaei M, Raeisi K, Vanhatalo S, Zappasodi F, Comani S, Tokariev A. Neonatal cortical activity organizes into transient network states that are affected by vigilance states and brain injury. Neuroimage Oct. 2023;279:120342. https://doi.org/10.1016/j.neuroimage.2023.120342.

[45] Bai Y, Belardinelli P, Ziemann U. Bihemispheric sensorimotor oscillatory network states determine cortical responses to transcranial magnetic stimulation. Brain Stimul Jan. 2022;15(1):167–78. https://doi.org/10.1016/j.brs.2021.12.002.

[46] Bai Y, Xuan J, Jia S, Ziemann U. TMS of parietal and occipital cortex locked to spontaneous transient large-scale brain states enhances natural oscillations in EEG. Brain Stimul Nov. 2023;16(6):1588–97. https://doi.org/10.1016/j.brs.2023.10.008.

[47] Metsomaa J, Belardinelli P, Ermolova M, Ziemann U, Zrenner C. Causal decoding of individual cortical excitability states. Neuroimage Dec. 2021;245:118652. https://doi.org/10.1016/j.neuroimage.2021.118652.

[48] Groppa S, et al. A practical guide to diagnostic transcranial magnetic stimulation: report of an IFCN committee. Clin Neurophysiol May 2012;123(5):858–82. https://doi.org/10.1016/j.clinph.2012.01.010.

[49] Westner BU, et al. A unified view on beamformers for M/EEG source reconstruction. Neuroimage Feb. 2022;246:118789. https://doi.org/10.1016/j.neuroimage.2021.118789.

[50] Tzourio-Mazoyer N, et al. Automated anatomical labeling of activations in SPM using a macroscopic anatomical parcellation of the MNI MRI single-subject brain. Neuroimage Jan. 2002;15(1):273–89. https://doi.org/10.1006/nimg.2001.0978.

[51] Colclough GL, Brookes MJ, Smith SM, Woolrich MW. A symmetric multivariate leakage correction for MEG connectomes. Neuroimage Aug. 2015;117:439–48. https://doi.org/10.1016/j.neuroimage.2015.03.071.

[52] Thomas Yeo BT, et al. The organization of the human cerebral cortex estimated by intrinsic functional connectivity. J Neurophysiol Sep. 2011;106(3):1125–65. https://doi.org/10.1152/jn.00338.2011.

[53] Gong G, et al. Mapping anatomical connectivity patterns of human cerebral cortex using in vivo diffusion tensor imaging tractography. Cerebr Cortex Mar. 2009;19(3):524–36. https://doi.org/10.1093/cercor/bhn102.

[54] Tewarie P, et al. Tracking dynamic brain networks using high temporal resolution MEG measures of functional connectivity. Neuroimage Oct. 2019;200:38–50. https://doi.org/10.1016/j.neuroimage.2019.06.006.

[55] Vidaurre D, Quinn AJ, Baker AP, Dupret D, Tejero-Cantero A, Woolrich MW. Spectrally resolved fast transient brain states in electrophysiological data. Neuroimage Feb. 2016;126:81–95. https://doi.org/10.1016/j.neuroimage.2015.11.047.
[56] O'Neill GC, Tewarie P, Vidaurre D, Liuzzi L, Woolrich MW, Brookes MJ. Dynamics of large-scale electrophysiological networks: a technical review. Neuroimage Oct. 2018;180:559–76. https://doi.org/10.1016/j.neuroimage.2017.10.003.
[57] Vidaurre D, et al. Discovering dynamic brain networks from big data in rest and task. Neuroimage Oct. 2018;180:646–56. https://doi.org/10.1016/j.neuroimage.2017.06.077.
[58] Marzetti L, et al. Towards real-time identification of large-scale brain states for improved brain state-dependent stimulation. Clin Neurophysiol Feb. 2024;158:196–203. https://doi.org/10.1016/j.clinph.2023.09.005.
[59] Kong RQ, et al. A network correspondence toolbox for quantitative evaluation of novel neuroimaging results Jun. 18, 2024. https://doi.org/10.1101/2024.06.17.599426.
[60] Quinn AJ, Vidaurre D, Abeysuriya R, Becker R, Nobre AC, Woolrich MW. Task-evoked dynamic network analysis through hidden Markov modeling. Front Neurosci Aug. 2018;12:603. https://doi.org/10.3389/fnins.2018.00603.
[61] Seedat ZA, et al. The role of transient spectral "bursts" in functional connectivity: a magnetoencephalography study. Neuroimage Apr. 2020;209:116537. https://doi.org/10.1016/j.neuroimage.2020.116537.
[62] Alonso S, Vidaurre D. Towards stability of dynamic FC estimates in neuroimaging and electrophysiology: solutions and limits. Janus 2023;20. https://doi.org/10.1101/2023.01.18.524539.
[63] Beckmann CF, DeLuca M, Devlin JT, Smith SM. Investigations into resting-state connectivity using independent component analysis. Philos. Trans. R. Soc. B Biol. Sci. May 2005;360(1457):1001–13. https://doi.org/10.1098/rstb.2005.1634.
[64] Klimesch W. Alpha-band oscillations, attention, and controlled access to stored information. Trends Cognit Sci Dec. 2012;16(12):606–17. https://doi.org/10.1016/j.tics.2012.10.007.
[65] Clayton MS, Yeung N, Cohen Kadosh R. The roles of cortical oscillations in sustained attention. Trends Cognit Sci Apr. 2015;19(4):188–95. https://doi.org/10.1016/j.tics.2015.02.004.
[66] Anderson KL, Ding M. Attentional modulation of the somatosensory mu rhythm. Neuroscience Apr. 2011;180:165–80. https://doi.org/10.1016/j.neuroscience.2011.02.004.
[67] Dixon ML, et al. Heterogeneity within the frontoparietal control network and its relationship to the default and dorsal attention networks. Proc Natl Acad Sci USA Feb. 2018;115(7). https://doi.org/10.1073/pnas.1715766115.
[68] Fox MD, Snyder AZ, Vincent JL, Corbetta M, Van Essen DC, Raichle ME. The human brain is intrinsically organized into dynamic, anticorrelated functional networks. Proc Natl Acad Sci USA Jul. 2005;102(27):9673–8. https://doi.org/10.1073/pnas.0504136102.
[69] Vossel S, Geng JJ, Fink GR. Dorsal and ventral attention systems: distinct neural circuits but collaborative roles. Neuroscientist Apr. 2014;20(2):150–9. https://doi.org/10.1177/1073858413494269.
[70] Aron AR, Robbins TW, Poldrack RA. Inhibition and the right inferior frontal cortex. Trends Cognit Sci Apr. 2004;8(4):170–7. https://doi.org/10.1016/j.tics.2004.02.010.
[71] Aron AR, Robbins TW, Poldrack RA. Inhibition and the right inferior frontal cortex: one decade on. Trends Cognit Sci Apr. 2014;18(4):177–85. https://doi.org/10.1016/j.tics.2013.12.003.
[72] Marzetti L, et al. Exploring motor network connectivity in state-dependent transcranial magnetic stimulation: a proof-of-concept study. Biomedicines Apr. 2024;12(5):955. https://doi.org/10.3390/biomedicines12050955.
[73] Yin S, Liu Y, Ding M. Amplitude of sensorimotor mu rhythm is correlated with bold from multiple brain regions: a simultaneous EEG-fMRI study. Front Hum Neurosci 2016;10(Jul). https://doi.org/10.3389/fnhum.2016.00364.
[74] Engel AK, Gerloff C, Hilgetag CC, Nolte G. Intrinsic coupling modes: multiscale interactions in ongoing brain activity. Neuron Nov. 2013;80(4):867–86. https://doi.org/10.1016/j.neuron.2013.09.038.
[75] Madsen KH, Karabanov AN, Krohne LG, Safeldt MG, Tomasevic L, Siebner HR. No trace of phase: corticomotor excitability is not tuned by phase of pericentral mu-rhythm. Brain Stimul Sep. 2019;12(5):1261–70. https://doi.org/10.1016/j.brs.2019.05.005.
[76] Rossi C, et al. A data-driven network decomposition of the temporal, spatial, and spectral dynamics underpinning visual-verbal working memory processes. Commun Biol Oct. 2023;6(1):1079. https://doi.org/10.1038/s42003-023-05448-z.
[77] Gohil C, et al. Mixtures of large-scale dynamic functional brain network modes. Neuroimage Nov. 2022;263:119595. https://doi.org/10.1016/j.neuroimage.2022.119595.
[78] Bai Y, Xuan J, Jia S, Ziemann U. TMS of parietal and occipital cortex locked to spontaneous transient large-scale brain states enhances natural oscillations in EEG. Brain Stimul Nov. 2023;16(6):1588–97. https://doi.org/10.1016/j.brs.2023.10.008.
[79] Cho S, Van Es M, Woolrich M, Gohil C. Comparison between EEG and MEG of static and dynamic resting-state networks. Hum Brain Mapp Sep. 2024;45(13):e70018. https://doi.org/10.1002/hbm.70018.
[80] Vinutha H, Yogananda BV. Advanced meta-learning techniques for inference of neural states under anesthetic conditions. In: *2024 international Conference on recent Advances in Science and engineering technology (ICRASET)*, B G Nagara, Mandya, India. IEEE; Nov. 2024. p. 1–8. https://doi.org/10.1109/ICRASET63057.2024.10895285.
[81] Liu Y, et al. Brain model state space reconstruction using an LSTM neural network. J Neural Eng Jun. 2023;20(3):036024. https://doi.org/10.1088/1741-2552/acd871.
[82] Wang Q, Liu F, Wan G, Chen Y. Inference of brain states under anesthesia with meta learning based deep learning models. IEEE Trans Neural Syst Rehabil Eng 2022;30:1081–91. https://doi.org/10.1109/TNSRE.2022.3166517.
[83] Alvi AM, Siuly S, Wang H. A long short-term memory based framework for early detection of mild cognitive impairment from EEG signals. IEEE Trans. Emerg. Top. Comput. Intell. Apr. 2023;7(2):375–88. https://doi.org/10.1109/TETCI.2022.3186180.
[84] Mittal A, Linderman S, Paisley J, Sajda P. Bayesian recurrent state space model for rs-fMRI. arXiv 2020. https://doi.org/10.48550/ARXIV.2011.07365.
[85] Sun S, et al. Resting-state dynamic functional connectivity in major depressive disorder: a systematic review. Prog Neuropsychopharmacol Biol Psychiatry Dec. 2024;135:111076. https://doi.org/10.1016/j.pnpbp.2024.111076.
[86] Wang S, et al. Transition and dynamic reconfiguration of whole-brain network in major depressive disorder. Mol Neurobiol Oct. 2020;57(10):4031–44. https://doi.org/10.1007/s12035-020-01995-2.
[87] Rossi C, et al. Impaired activation of the prefrontal executive network during working memory processing in multiple sclerosis. Dec 2023;27. https://doi.org/10.1101/2023.12.22.573051.
[88] Sack AT, et al. Target engagement and brain state dependence of transcranial magnetic stimulation: implications for clinical practice. Biol Psychiatry Mar. 2024;95(6):536–44. https://doi.org/10.1016/j.biopsych.2023.09.011.
[89] Zrenner B, et al. Brain oscillation-synchronized stimulation of the left dorsolateral prefrontal cortex in depression using real-time EEG-triggered TMS. Brain Stimul Jan. 2020;13(1):197–205. https://doi.org/10.1016/j.brs.2019.10.007.
[90] Fleury M, Figueiredo P, Vourvopoulos A, Lécuyer A. Two is better? combining EEG and fMRI for BCI and neurofeedback: a systematic review. J Neural Eng Oct. 2023;20(5):051003. https://doi.org/10.1088/1741-2552/ad06e1.
[91] Gotman J, Kobayashi E, Bagshaw AP, Bénar C, Dubeau F. Combining EEG and fMRI: a multimodal tool for epilepsy research. J Magn Reson Imag Jun. 2006;23(6):906–20. https://doi.org/10.1002/jmri.20577.
[92] Peters JC, Reithler J, Graaf TAD, Schuhmann T, Goebel R, Sack AT. Concurrent human TMS-EEG-fMRI enables monitoring of oscillatory brain state-dependent gating of cortico-subcortical network activity. Commun Biol Jan. 2020;3(1):40. https://doi.org/10.1038/s42003-020-0764-0.